

## Supplementary Information

# Interfacial Catalysis and Lignin Nanoparticles for Strong Fire- and Water-resistant Composite Adhesives

K. Alexander Henn, Susanna Forssell, Antti Pietiläinen, Nina Forsman, Ira Smal, Paula Nousiainen, Rahul Prasad Bangalore Ashok, Pekka Oinas, Monika Österberg

## Contents

Supplementary Note 1: Method for examining epoxidation reaction speed .....	2
Supplementary Note 2: Epoxidation Reaction Details .....	2
Supplementary Note 3: Structural Characterization .....	4
FTIR analysis .....	4
<sup>1</sup> H-NMR analysis .....	8
HSQC analysis .....	8
<sup>31</sup> P-NMR analysis .....	9
Epoxidation reaction progress (FTIR, <sup>1</sup> H NMR and HSQC) .....	9
Supplementary Note 4: Mechanical Characterization .....	12
The effect of adhesive spread .....	12
Mode of failure .....	13
Adhesive cured structure .....	15
Supplementary Note 5: Thermal Characterization .....	20
Supplementary Note 6: Lignin Particle Size and Surface charge .....	21
Supplementary Note 7: Estimation of operating cost .....	22
Supplementary Note 8: Life cycle assessment .....	22
References .....	25

## Supplementary Note 1: Method for examining epoxidation reaction speed

The exponential increase in temperature was used as indication for reaction initiation. The progress of the reaction was further examined using a combination of FTIR, <sup>1</sup>H NMR and HSQC. This test was done with a larger amount of excess epichlorohydrin and a lower lignin concentration. The decreased lignin-concentration was thought to lead to less homopolymerization and make NMR analysis more precise. First, 1 gram of lignin was dissolved in 9 g 1 M NaOH. The temperature of the lignin solution was 25 °C. Then, 3 ml of the lignin solution was added to 7 ml epichlorohydrin at 45 °C while stirring efficiently with a magnet stirrer. The beaker containing the epichlorohydrin was insulated with one layer of plastic foam (ca. 1 cm thick) and two layers of aluminum foil on the sides and two on top as a lid to minimize cooling or heat loss. The temperature dropped to ca. 37 °C when the lignin solution had been added, but quickly increased according to Fig. S3a. Three identical samples were made; one reacted for 3 minutes, one reacted for 6 minutes, and the third for 9 minutes. The samples were precipitated using 100 ml ice cold acetone, and the traces of epichlorohydrin were extracted with two pentane washes. Then, 2 ml deionized water was added to the samples, and the pH was adjusted to 9.5 using 0.1 M HCl. The yield of the samples reacted for 3 min, 6 min and 9 min was 86%, 92%, and 102 %, respectively. The loss of material occurred during the acetone precipitation. This loss could be avoided with an additional centrifugation step to obtain the suspended phase. The samples were analyzed using FTIR, <sup>1</sup>H-NMR, and HSQC. The results are discussed in Supplementary Note 4.

## Supplementary Note 2: Epoxidation Reaction Details

The conditions were found by analyzing the temperature at which a clear increase in temperature was observed. The increase in temperature was seen at approximately 39.5 °C, but was significantly faster above 40 °C. The exothermic effect was leveled out after ~3.5 minutes (Fig. S3a), indicating that the available lignin had been reacted with epichlorohydrin. By increasing the concentration of lignin, the temperature increase is more intense. To avoid excessively high temperatures (above 55 °C), the lignin was added in small portions (Fig. S3b). In larger scale, this process could be mimicked by a continuous flow reactor to maintain a temperature above 45 °C without needing to provide cooling or heating. The epichlorohydrin and the lignin solution were clearly in separate phases in the beginning of the reaction, but then seemed to combine into one phase. Microscopy analysis nevertheless revealed that the phases do not combine – the reaction proceeds as an emulsion (Fig. S2). Notably, the emulsion was only oil-in-water and formed only in the presence of lignin. This suggests that lignin dissolved in the water phase acts as emulsifier.

The reaction was stopped by solvent exchange rather than acidification, which left the product highly alkaline. Acidification would result in the precipitation of one soluble product and one precipitated product, which is not desired. Still, the alkaline product had a low shelf-life and cured by itself in less than a day at room temperature. This could be due to alkaline hydrolysis via an S<sub>N</sub>2 reaction (Fig. S11).<sup>1</sup>

Nearly neutral epoxidized kraft lignin (EKL) solutions however, remained runny even when stored at room temperature for a few days and could still be spread without difficulty after a week. The EKL remained both soluble and stable in pH levels between ca. 10 – 8.5.

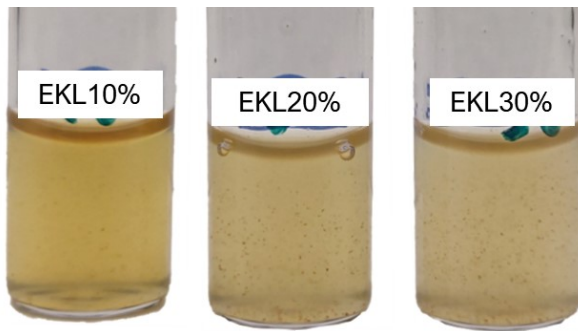


Fig. S1. Diluted solutions of EKL made using different initial lignin concentrations. Aggregates are visible especially in EKL20% and EKL30%.

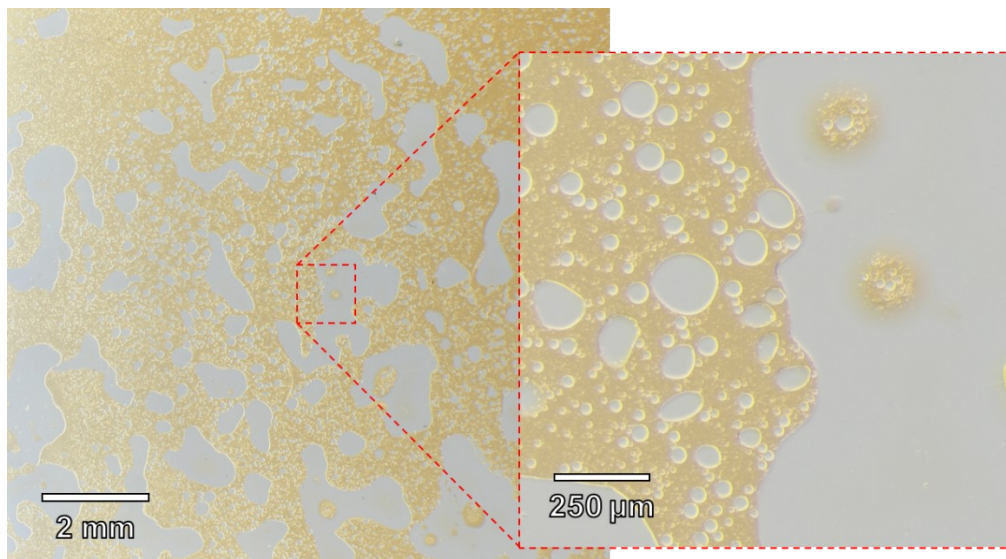


Fig. S2. Microscopy image of lignin-stabilized epichlorohydrin (clear phase) O/W droplets in lignin solution (light brown phase). This sample was isolated 9 minutes after the initiation of the epoxidation. The reaction was performed with 3 ml 10 wt.% lignin solution and 7 ml epichlorohydrin.

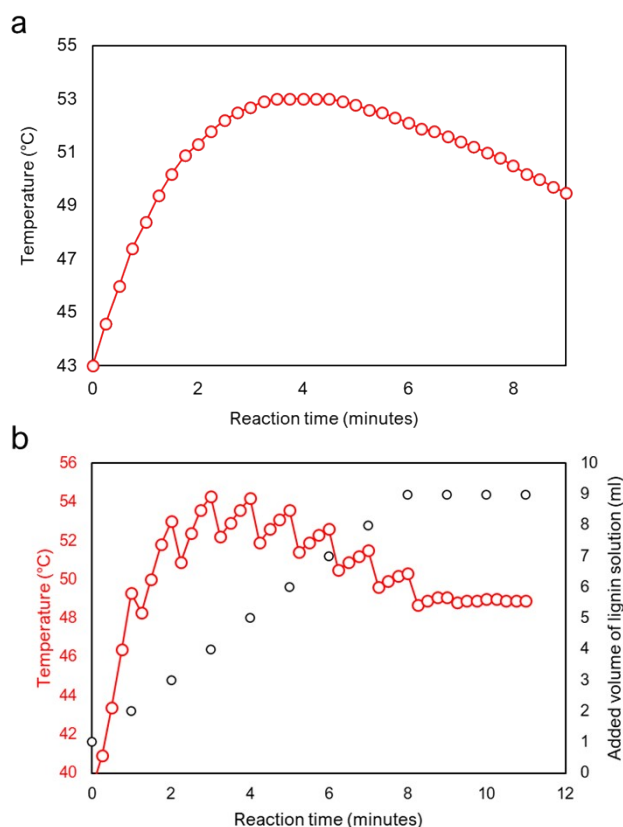


Fig. S3. Heat change of epoxidation reaction. (a) Heat change of 3 ml 10 wt.% lignin solution in 7 ml epichlorohydrin. (b) Heat change of 10 wt.% lignin solution added in 1 ml portions to 7 ml epichlorohydrin.

### Supplementary Note 3: Structural Characterization

#### FTIR analysis

The most important difference between the FTIR spectra of EKL and kraft lignin (KL) in this context is the presence of the oxirane band at  $906\text{ cm}^{-1}$ . Other structural differences are nevertheless also relevant, e.g. to evaluate the ratio of non-polar to polar structures which can provide catalytic action.<sup>1</sup> An increase in methylene groups is expected as the grafted epoxy groups contain two  $\text{CH}_2$  groups. These remain visible despite homopolymerization, in contrast to the epoxy group which is consumed. The ratio between methylene and epoxy groups can therefore be used as comparative indication of success when comparing different batches with each other. These bands were used to determine how the reaction time affected the product. Reaction times of 30 minutes caused a strong band at  $1360\text{ cm}^{-1}$ , which seemed to derive from aldehyde groups. The mechanism for the formation of aldehydes in the reaction is unknown but could stem from the deprotonation of the glycerol bridge created by homopolymerization. The ether band at  $1206\text{ cm}^{-1}$  was also more intense in the 30 minute-epoxidized lignin, which is a sign of homopolymerization. Table S1 presents structural components in lignin and their corresponding IR absorption wavenumbers. When comparing very short epoxidation reaction, it was observed that epoxidation still occurs after 3 minutes but has already slowed down at 6 minutes of reaction (Fig. S6b). The reaction progress is further discussed in the last part of this section. FTIR was

also used to determine differences between acidified and solvent-exchanged EKL and the purity of recovered epichlorohydrin after the epoxidation reaction (Fig. S7). The spectra of solvent-exchanged EKL was in the middle of the dissolved and solid phases in acidified EKL, suggesting that structures resembling both phases were present.

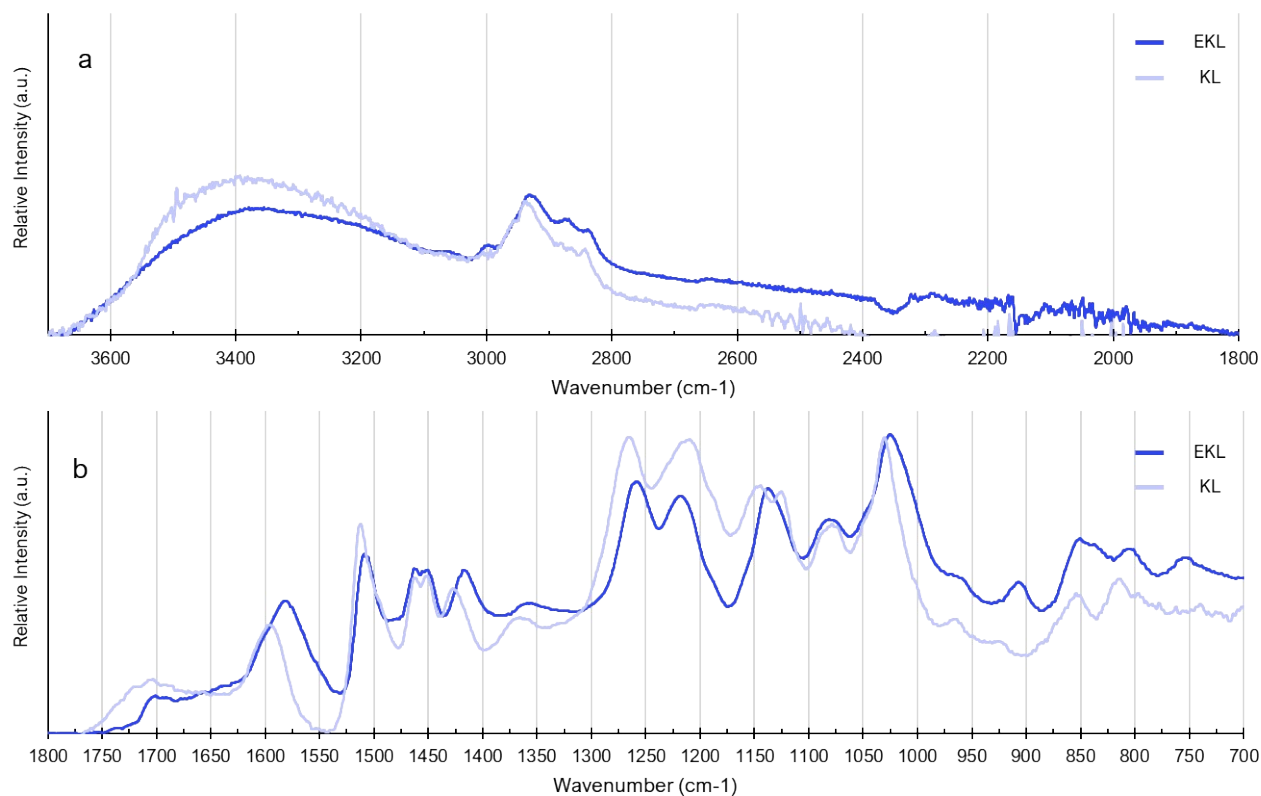


Fig. S4. FT-IR absorption spectra of epoxidized kraft lignin (EKL) and kraft lignin (KL). (a) Region between wavenumbers 3700 – 1800 cm<sup>-1</sup>, normalized between 3700 – 1800 cm<sup>-1</sup>. (b) Region between wavenumbers 1800 – 700 cm<sup>-1</sup>, *min-max* normalized between 1800 – 700 cm<sup>-1</sup>.

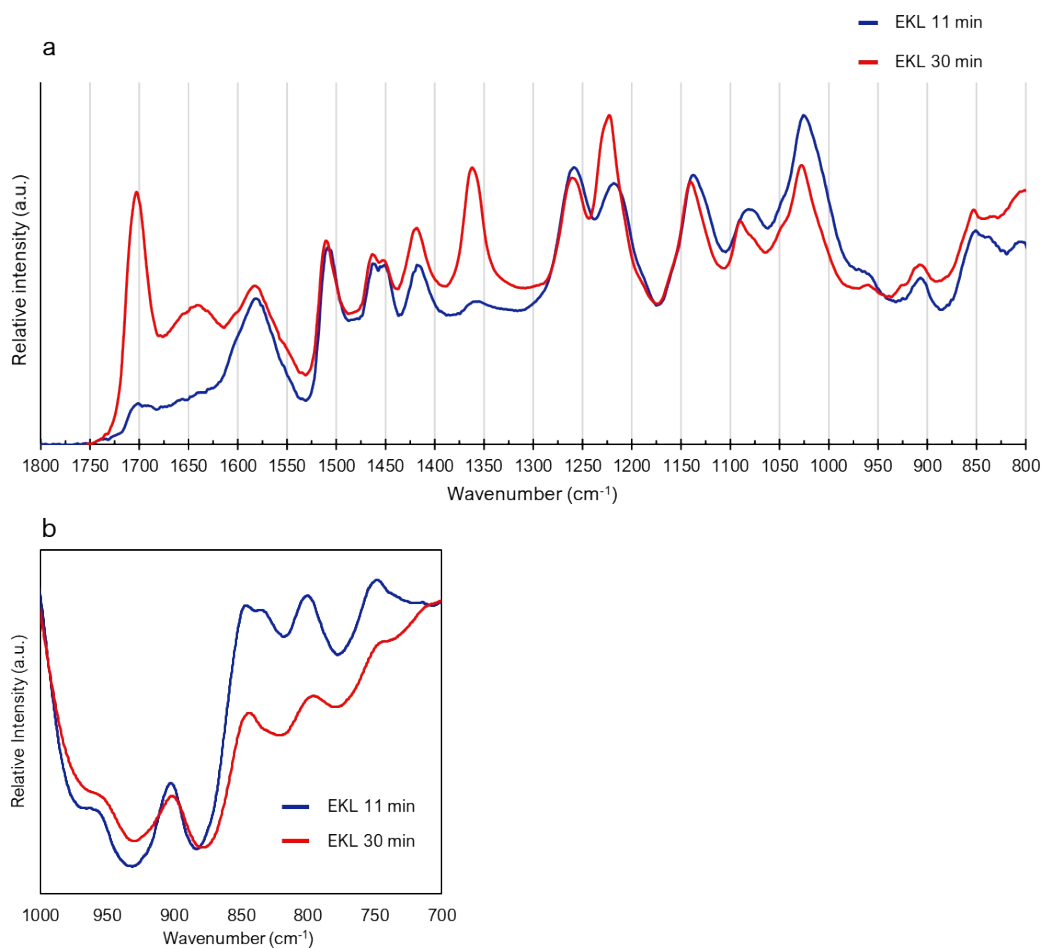


Fig. S5. FTIR spectra of EKL from an 11-minute reaction and a 30-minute reaction. (a) Fingerprint region *min-max* normalized between 1800 – 800 cm<sup>-1</sup>. (b) Spectrum with focus on epoxy band at ~906 cm<sup>-1</sup>, linearly baseline-corrected according to area between 930 – 890 cm<sup>-1</sup> and normalized using minimum and maximum values between 1000 – 890 cm<sup>-1</sup>.

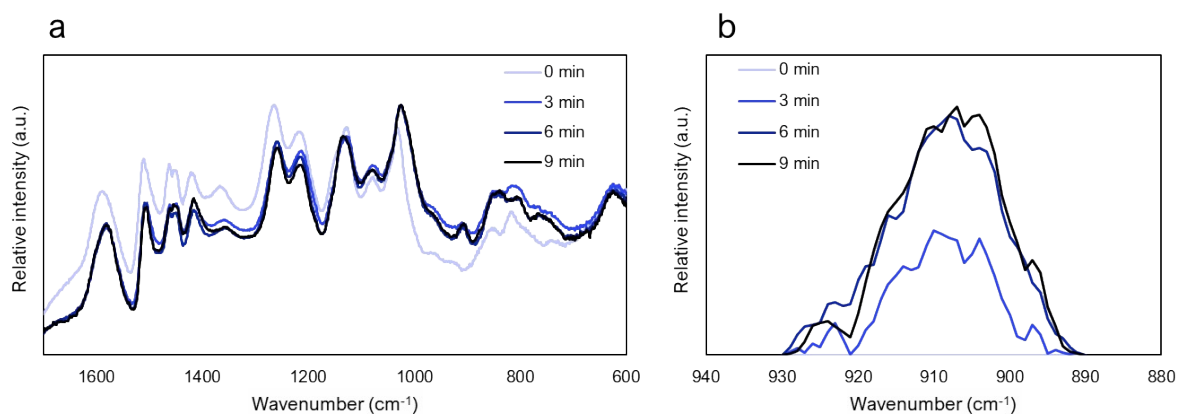


Fig. S6. Effect of epoxidation reaction time on lignin IR absorption. (a) FTIR fingerprint region of unmodified lignin (0 min) and lignin epoxidized for different durations (3 – 9 minutes). The spectra were *min-max* normalized between 4000 – 600 cm<sup>-1</sup>. (b) The intensity of the epoxy band (930 – 890 cm<sup>-1</sup>) of lignin epoxidized with different reaction times. The spectra were *min-max* normalized between 1024 and 890 cm<sup>-1</sup>, and then integrated above a linear baseline from the points between 930 – 890 cm<sup>-1</sup>. The integrated signal values are found in Fig. S12a.

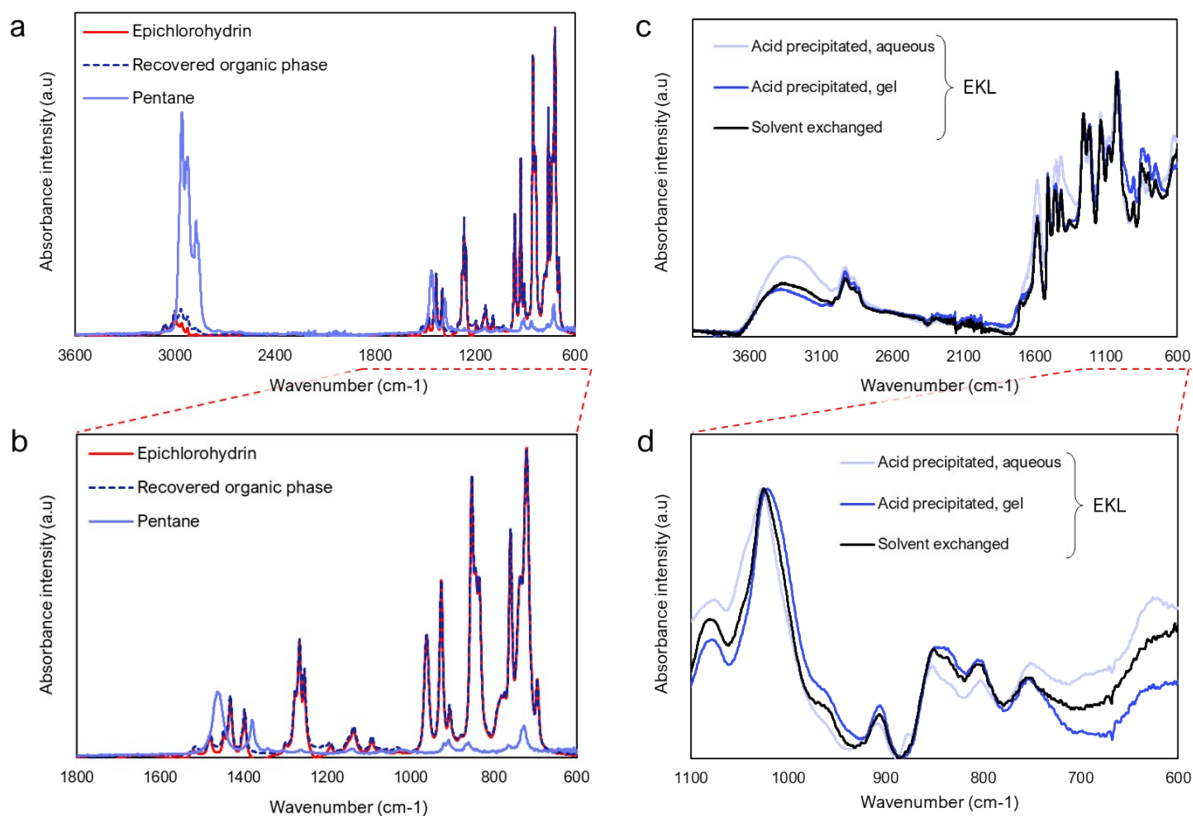


Fig. S7. Quenching methods, their effect on the product, and their chemical recoverability. (a) The full spectra and (b) the fingerprint region of solvent-extracted epichlorohydrin (recovered organic phase) compared to pure epichlorohydrin. (c) The full spectra and (d) the fingerprint region of acid precipitated and solvent-exchanged EKL. The spectra in (a – c) were *min-max* normalized between 4000 – 600 cm<sup>-1</sup>, and the spectra in (c) was *min-max* normalized between 1024 – 890 cm<sup>-1</sup>.

Table S1. Absorption signals of varying lignin structures and notes regarding EKL and KL comparison.

Wavenumber (cm <sup>-1</sup> )	Structure	Reference
3700 – 3050	Hydrogen bonding, electrostatic bonding, stretching vibrations.	2-4
3000 – 2750	Methyl groups (CH <sub>3</sub> ) and methylene (CH <sub>2</sub> ). Symmetrical and asymmetrical C-H stretching.	2-4
1700	Unconjugated carbonyl/carboxyl stretching	3,4
1625 – 1550	Symmetric aromatic skeletal vibrations	3,4
1510	Unsymmetric aromatic skeletal vibrations	2-4
1480	Asymmetrical CH <sub>2</sub>	5
1466	Asymmetric C-H deformation	4
1458	Asymmetric O-CH <sub>3</sub> and O-CH deformation	3,4
1424	Aromatic skeletal vibrations combined with C-H in plane deformation	2,4
1425 – 1390	Symmetrical CH <sub>2</sub> bending	5
1398	Alkene, C=C-H in-plane bending	5
1263	Aromatic ring breathing with C=O, C-C, and C-O stretch	2,3,6
1206	Ether linkages	7
1143 and 1123	Guaiacyl unit C-H in plane deformation	3,4
1076	C-O deformation from secondary alcohols and aliphatic ethers	4
1030	Aromatic C-H deformation	2,4
906	C-O stretching form oxirane (epoxy) ring.	2

### *<sup>1</sup>H-NMR analysis*

EKL and KL had similar spectra, except for the epoxy signal at 2.65 ppm.<sup>8</sup> The results are presented in Fig. S8. The EKLs spectra was slightly smoothed out because of the increased molecular size. It is unclear how this affects the ability to quantify structural features as it may weaken the obtained signals. The ratios of structural features could nevertheless be compared in HSQC, which is discussed in the following section.

### *HSQC analysis*

HSQC analysis was used to compare basic structural elements in kraft lignin and EKL.<sup>9</sup> The regions of interest and the corresponding structures are presented in Fig. S10 and Table S3. The epoxy signals were compared to methoxy signals to calculate the epoxy/methoxy ratio. For a nine-minute reaction following the procedure described in Supplementary Note 1:, this value was ca. 0.6 mol/mol, corresponding to an epoxy index (EI) of 2.6 mmol/g. For an 11-minute reaction with regular addition of lignin solution the ratio was 0.54 mol/mol, which corresponds to an EI of ca. 2.3 mmol/g.

### <sup>31</sup>P-NMR analysis

<sup>31</sup>P NMR was used to analyze the hydroxyl groups content after epoxidation. Aliphatic hydroxyl groups are not as reactive as phenolic hydroxyl groups, which is why most aliphatic hydroxyl groups remain after epoxidation. A new aliphatic signal at 146 ppm was also seen. This signal corresponded from the epoxy ring, which can react with the phosphitylation agent.<sup>8,10</sup> The phenolic hydroxyl groups had decreased from 3.9 mmol/g to only 0.5 mmol/g. The carboxylic groups had been reduced slightly in EKL. The presence of aliphatic and carboxylic groups may explain the good solubility of EKL in water, despite a large amount of hydroxyl groups, which are relatively polar, had been replaced with the relatively non-polar epoxy group. The results are presented in Table S2 and Fig. S9.

### Epoxidation reaction progress (FTIR, <sup>1</sup>H NMR and HSQC)

The samples obtained from 3 – 9 minutes epoxidations in excess epichlorohydrin, following the method described in Supplementary Note 1:, were used to determine the progress of the epoxidation reaction at the very first minutes. The progress was evaluated by combining results from FTIR, <sup>1</sup>H NMR and HSQC. All methods showed a similar trend: the epoxidation reaction proceeded fastest the first 3 minutes, and then slowed down between 3 – 6 minutes. Still, the EI values obtained from <sup>1</sup>H NMR were lower than those based on epoxy/methoxy ratios obtained in HSQC. This is likely because of decreased signal intensity of EKL caused by the relatively large molecular size. The methoxyl content of the lignin used in this study was characterized previously.<sup>11,12</sup> These results are presented in Fig. S12.

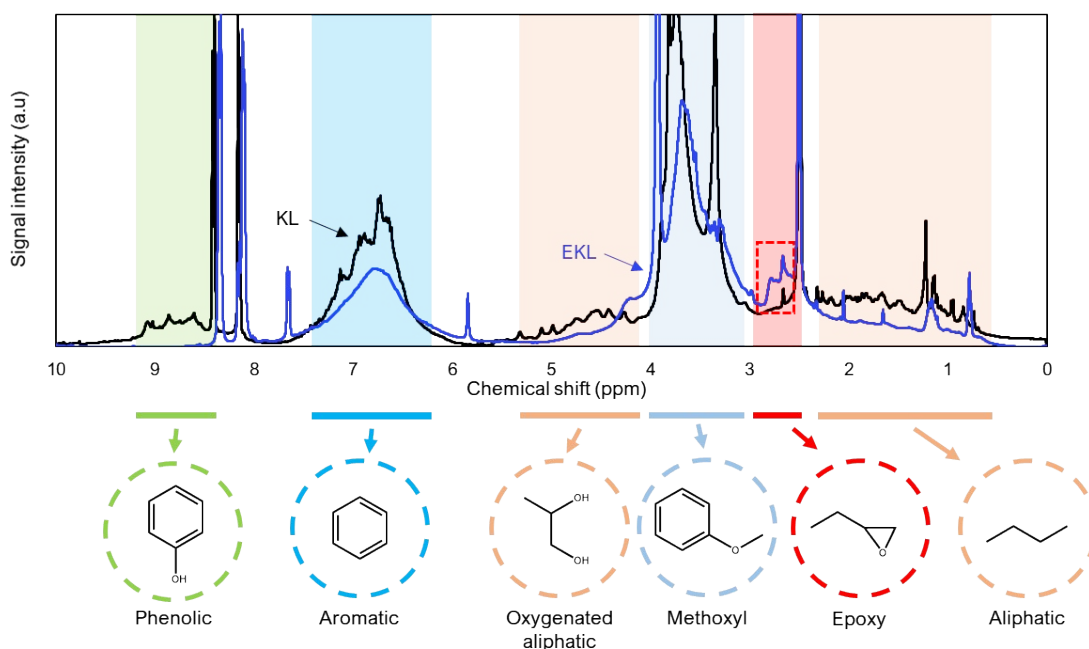


Fig. S8. <sup>1</sup>H-NMR spectra of kraft lignin (KL) and epoxidized kraft lignin (EKL). Regions showing hydroxyl-, aromatic-, aliphatic-, methoxyl-, and epoxide-structures are highlighted. The signal from the epoxy group is further highlighted in the dotted red square.

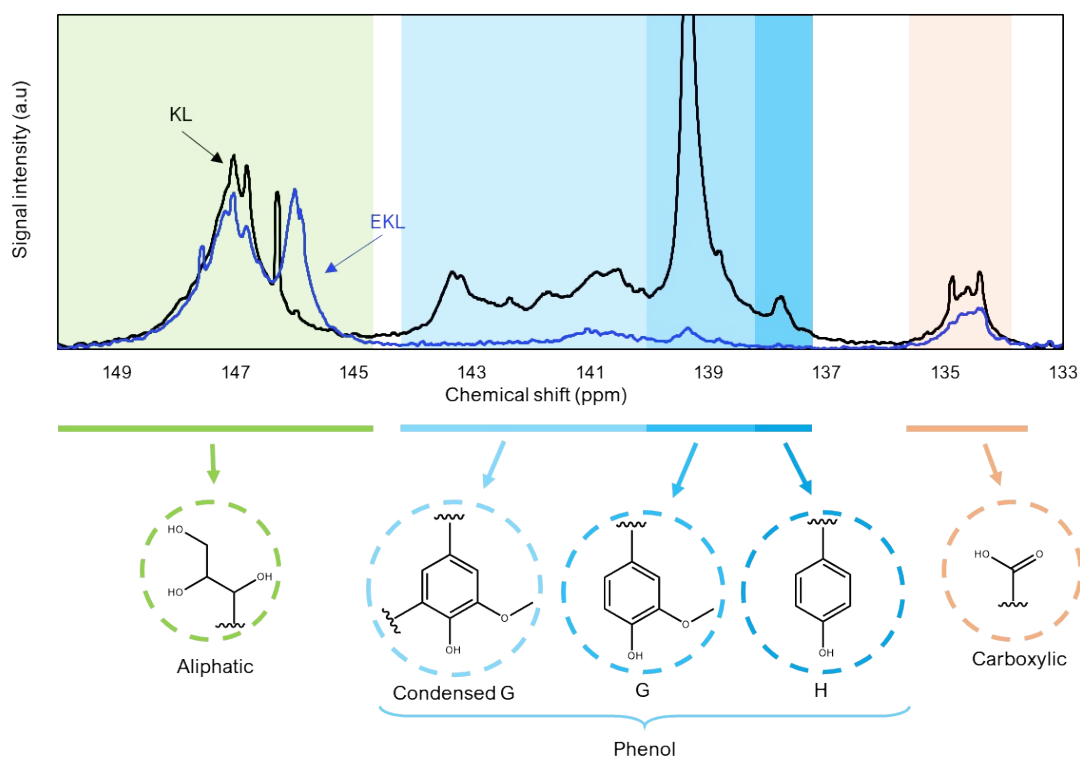


Fig. S9.  $^{31}\text{P}$ -NMR spectra of kraft lignin (KL) and epoxidized kraft lignin (EKL).<sup>13</sup> Regions showing aliphatic hydroxyl groups, condensed and non-condensed guaiacyl and 4-hydroxyphenyl phenolic hydroxyl groups and carboxylic hydroxyl groups highlighted.

Table S2. Hydroxyl group content of epoxidized kraft lignin (EKL) and kraft lignin (KL).

Hydroxyl type	EKL	KL	EKL/KL
	(mmol/g)	(mmol/g)	(%)
Aliphatic	2.15	2.01	110
Phenolic	0.49	3.91	12
Carboxylic	0.28	0.46	62
<b>Total</b>	<b>2.92</b>	<b>6.37</b>	<b>62</b>

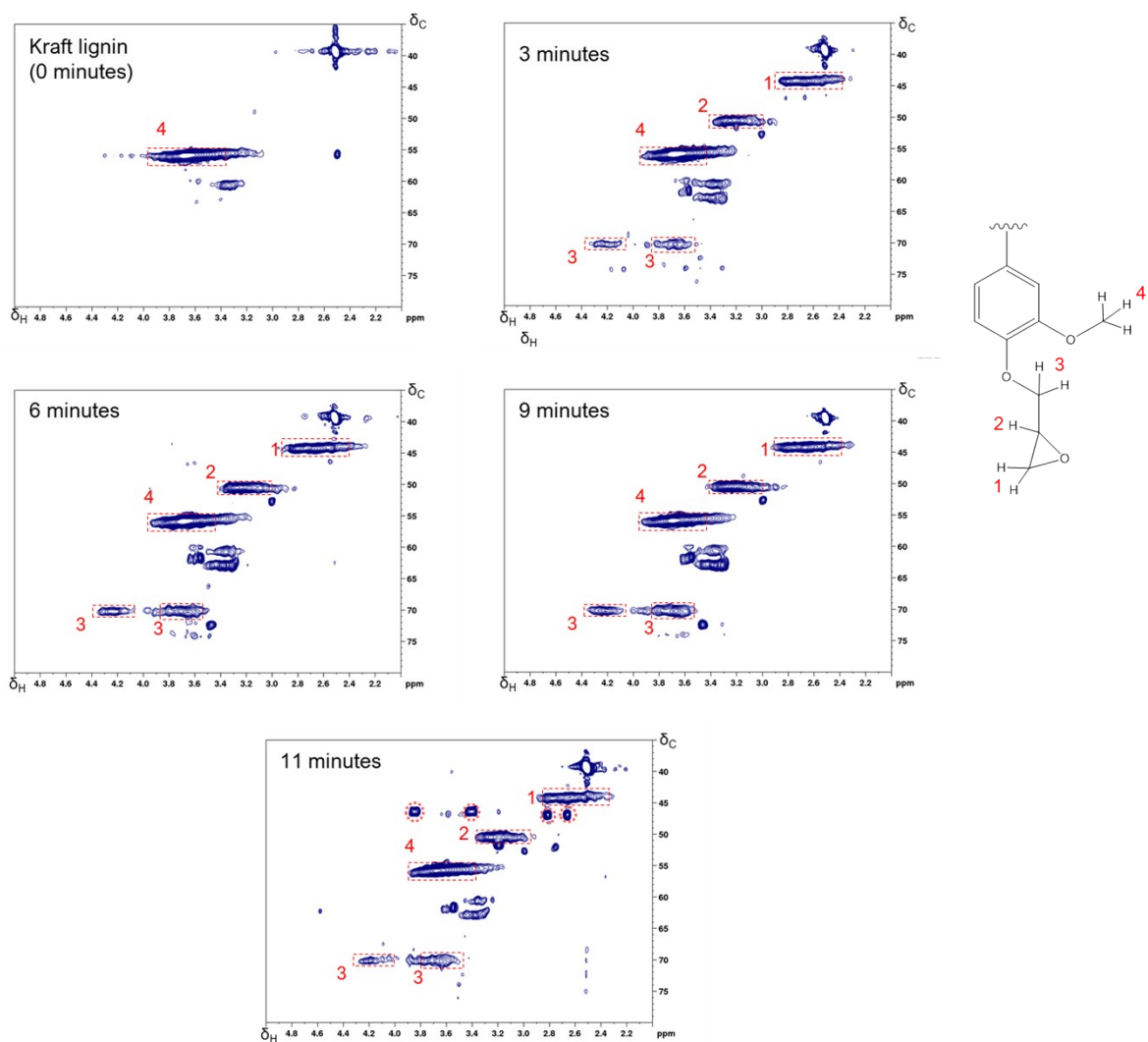


Fig. S10. HSQC spectra of epoxidized lignin prepared with different reaction times and the corresponding structures. The red dotted circles in the 11 minute epoxidized lignin are derived from residual epichlorohydrin.

Table S3. Intervals for integrated HSQC spectra. Numbers in brackets correspond to the structure shown in Fig. S10.

Structure	$\delta_H$ (ppm)	$\delta_C$ (ppm)
Epoxy (1)	2.67	44.3
Epoxy (2)	3.26	50.47
Epoxy (3)	4.23, 3.69	70.21, 70.28
Methoxyl (4)	3.68	55.86

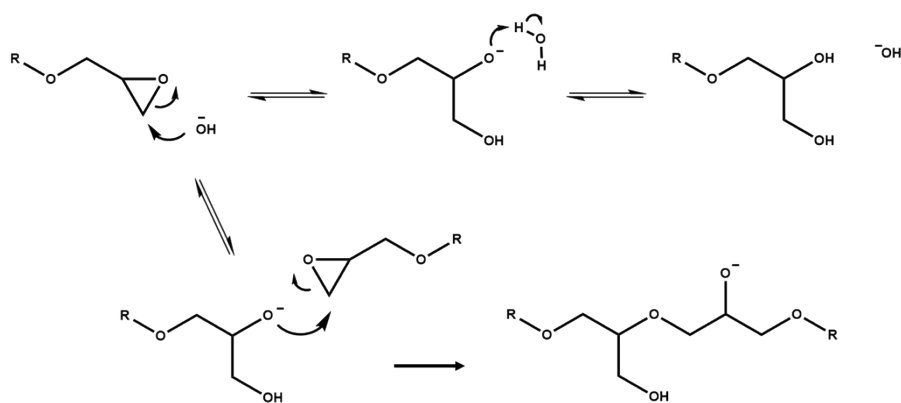


Fig. S11. Proposed mechanism of oxirane ring opening through  $S_N2$  reaction, leading either to the formation of new hydroxyl groups or polymerization in alkaline solutions.

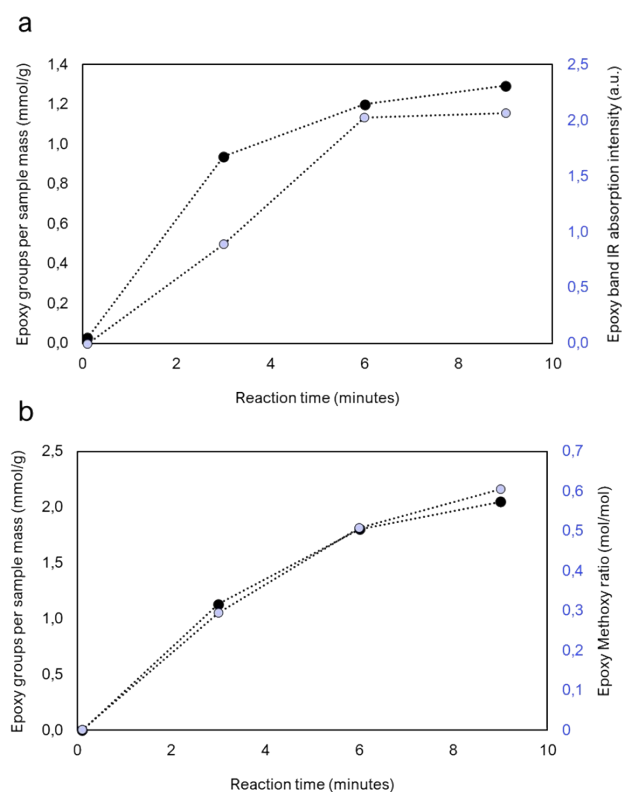


Fig. S12. The progress of the epoxidation reaction at the first 9 minutes. (a) Epoxy content determined by  $^1\text{H}$  NMR (dark circles) compared to integrated FTIR spectra (Fig. S6b) between  $930 - 810\text{ cm}^{-1}$  (light circles). (b) Epoxy index determined by epoxy-methoxy ratio (dark circles) and epoxy-methoxy ratio (light circles) determined by HSQC. The epoxy methoxy ratio was obtained by comparing integrals of areas 1 and 4 in Fig. S10 and the methoxyl content was corrected for the increased mass due to the grafting of epoxy.

## Supplementary Note 4: Mechanical Characterization

### *The effect of adhesive spread*

Both very thick and thin layers of adhesive were evaluated ( $50 - 650\text{ g/m}^2$ ). It was concluded that thin layers need less time to cure and therefore can provide higher strength with lower curing temperatures and shorter curing times. As the adhesive likely cures from the top and bottom towards the middle,

insufficient curing most likely leads to weak structures in the middle, especially when very thick layers are used. However, the highest adhesive strengths were obtained from samples with spreads above 350 g/m<sup>2</sup>, when the hot-press time and temperature was long and high enough. Still, strengths over 10 MPa could be achieved with spreads below 150 g/m<sup>2</sup>.

Wood failure did not always correlate with strength in samples with very thick spreads. It could be that the adhesive is not always able to fully absorb into the wood when thick layers are used, which leads to a relatively thick adhesive layer between the wood samples. If this layer breaks before the wood-fibers, no wood failure is observed despite achieving high adhesive strengths.

#### *Mode of failure*

The mode of failure is important to take into consideration when discussing the strength of wood adhesives. If the adhesive is stronger than the wood itself, the wood fibers in contact with the adhesive are ripped off. The adhesive's strength therefore does not only depend on the strength of the adhesive but also its penetration into the wood, in other words, the amount wood fibers that are in contact with the adhesive. The EKL+LNP adhesives strength and degree of wood failure showed some correlation when using adhesive spreads below 200 g/m<sup>2</sup> (Fig. S13). Wood failure was less common in samples with spreads above 200 g/m<sup>2</sup>, except in samples cured at 160 °C. It was shown that higher spreads required higher temperatures or longer curing times to fully cure, which partially explains the deviances. In samples soaked with water, only fibers at the outmost surface of the samples showed evidence of wood failure. To avoid the use of fossil-based curing agents, improving the penetration depth could increase the wet strength. The penetration was analyzed by light microscopy and shown to be approximately 100 ~ 120 μm (Fig. S14).

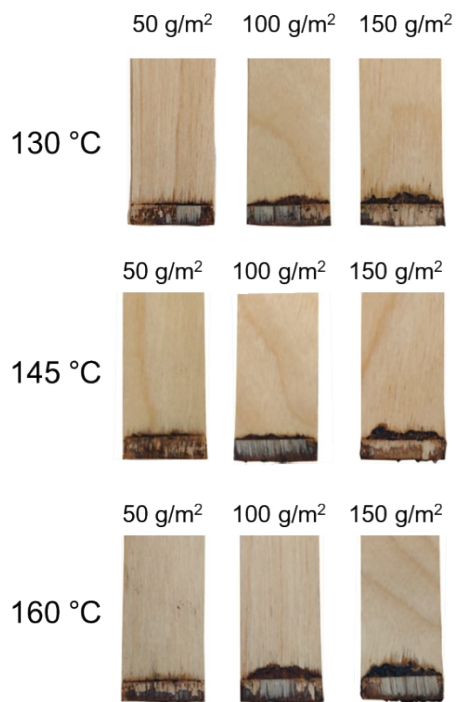


Fig. S13. Samples adhered with EKL: LNP after tensile testing showing varying degrees of wood failure. All samples were pressed for 5 minutes.

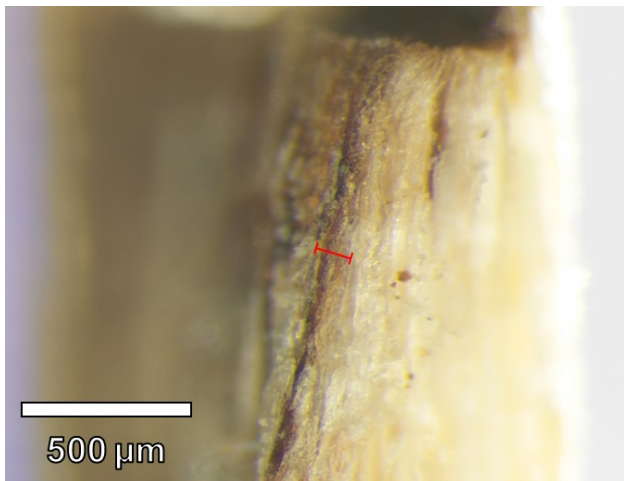


Fig. S14. Microscopy image showing depth of EKL+LNP penetration into wood. The length of the red line is 106 μm.

### Adhesive cured structure

The adhesives structure after being cured provides information about the interaction between LNPs and EKL. LNPs were clearly visible in EKL: LNP composite adhesive. The EKL:LNP composite was slightly more even overall. Cured EKL seemed somewhat grainy, which could increase brittleness.

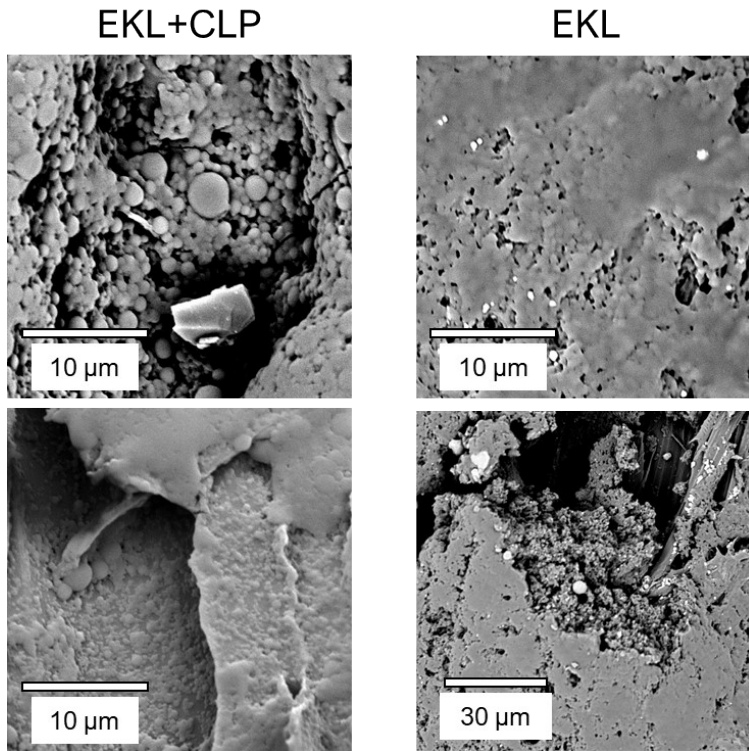


Fig. S15. Cured adhesives of EKL+LNP and EKL on wooden substrates.

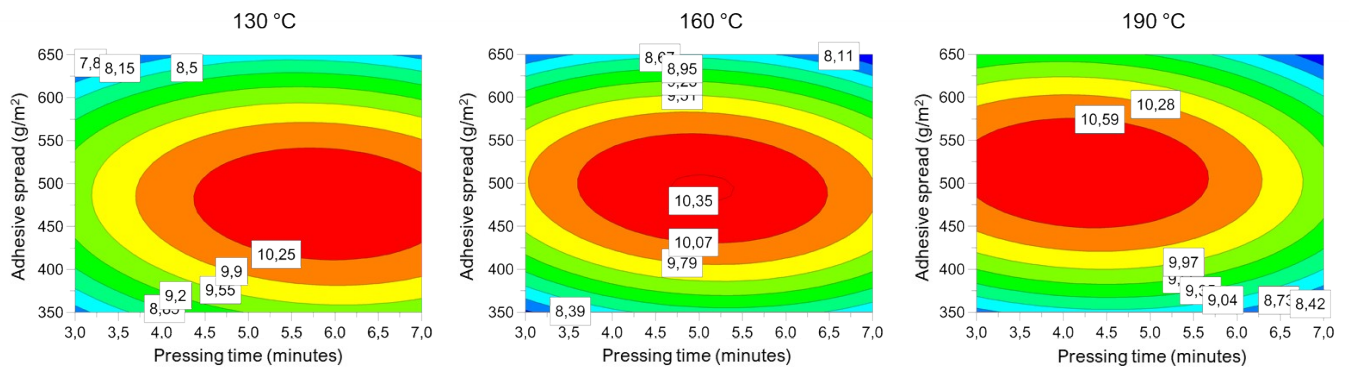


Fig. S16. Strength of EKL+LNP adhesives in model with expanded temperatures and curing times.

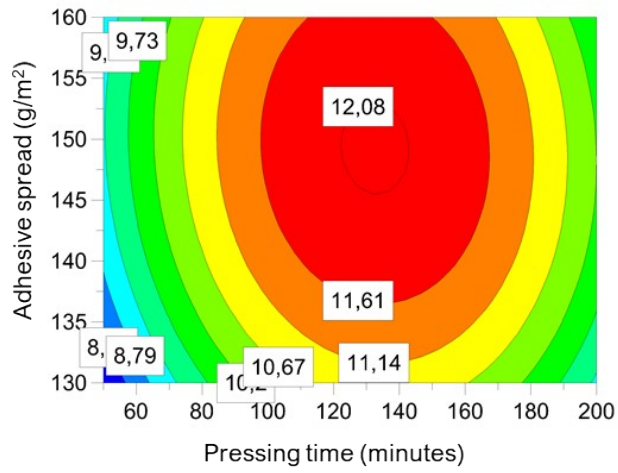


Fig. S17. Strength of EKL+LNP adhesives with low adhesive spreads. All samples were cured for 5 minutes at 145 °C.



Fig. S18. EKL+LNP adhesive lifting 10 kg. The sample had a joint area of 1 cm<sup>2</sup> and was glued with a spread of 100 g/m<sup>2</sup> and was hot pressed at 130 °C for 5 minutes. The water jugs contained about 5 liters each and weighed exactly 10.0 kg in total. A video of lifting the jugs from the ground can be found in the supplementary video.

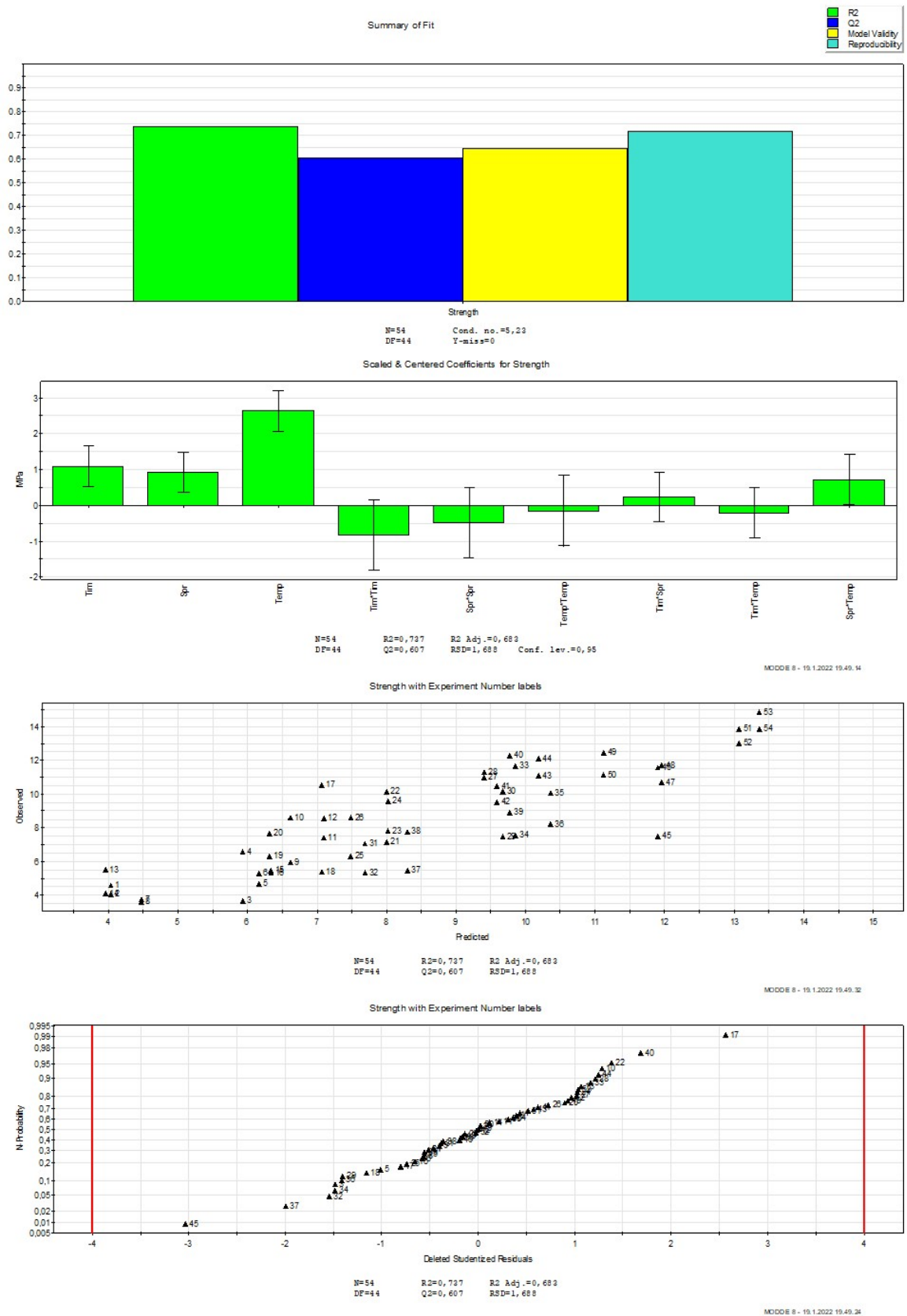


Fig. S19. Summary plot, coefficient plot, predicted versus occurred plot, and residual plot of Model 1.

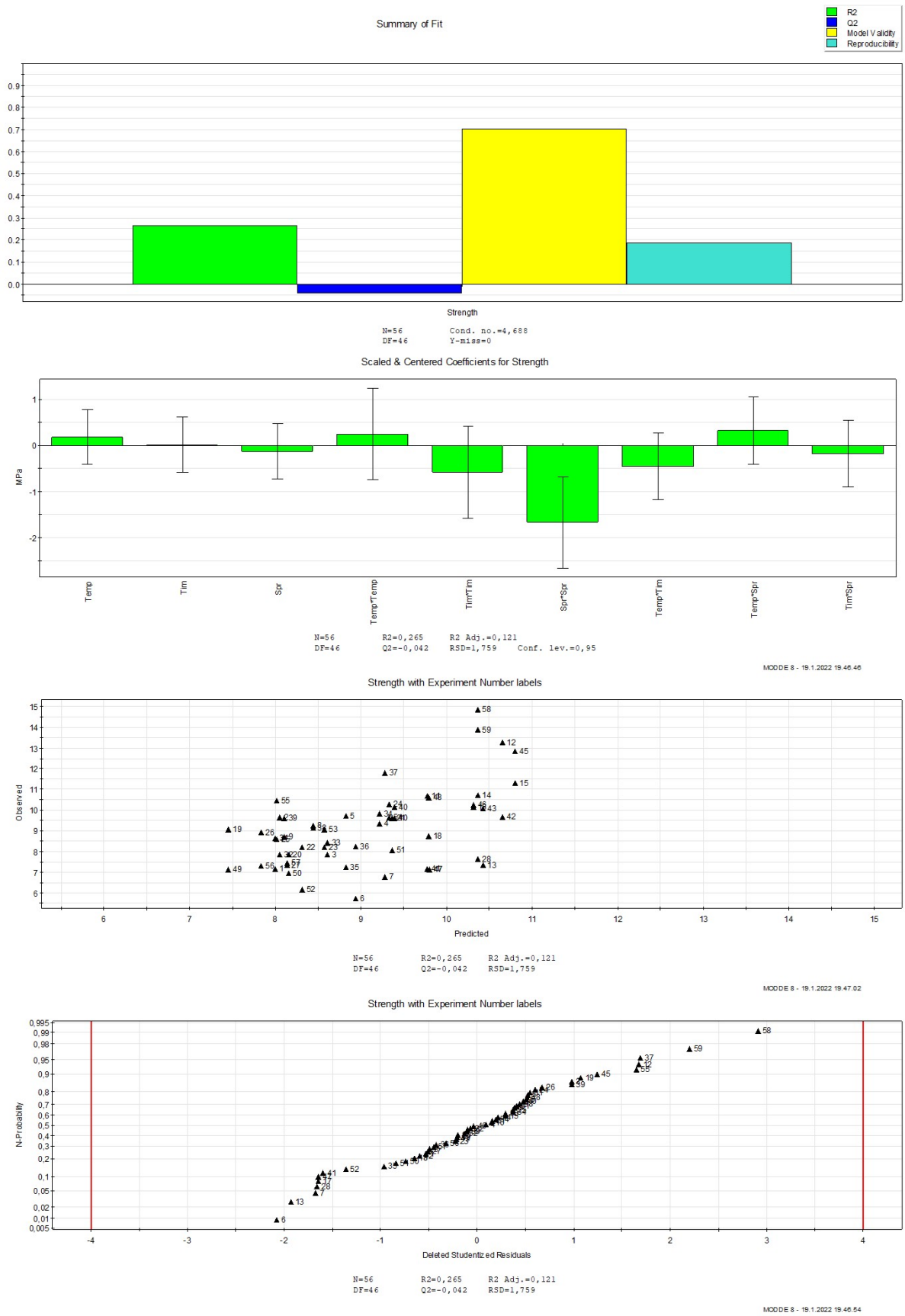


Fig. S20. Summary plot, coefficient plot, predicted versus occurred plot, and residual plot of Model 2.

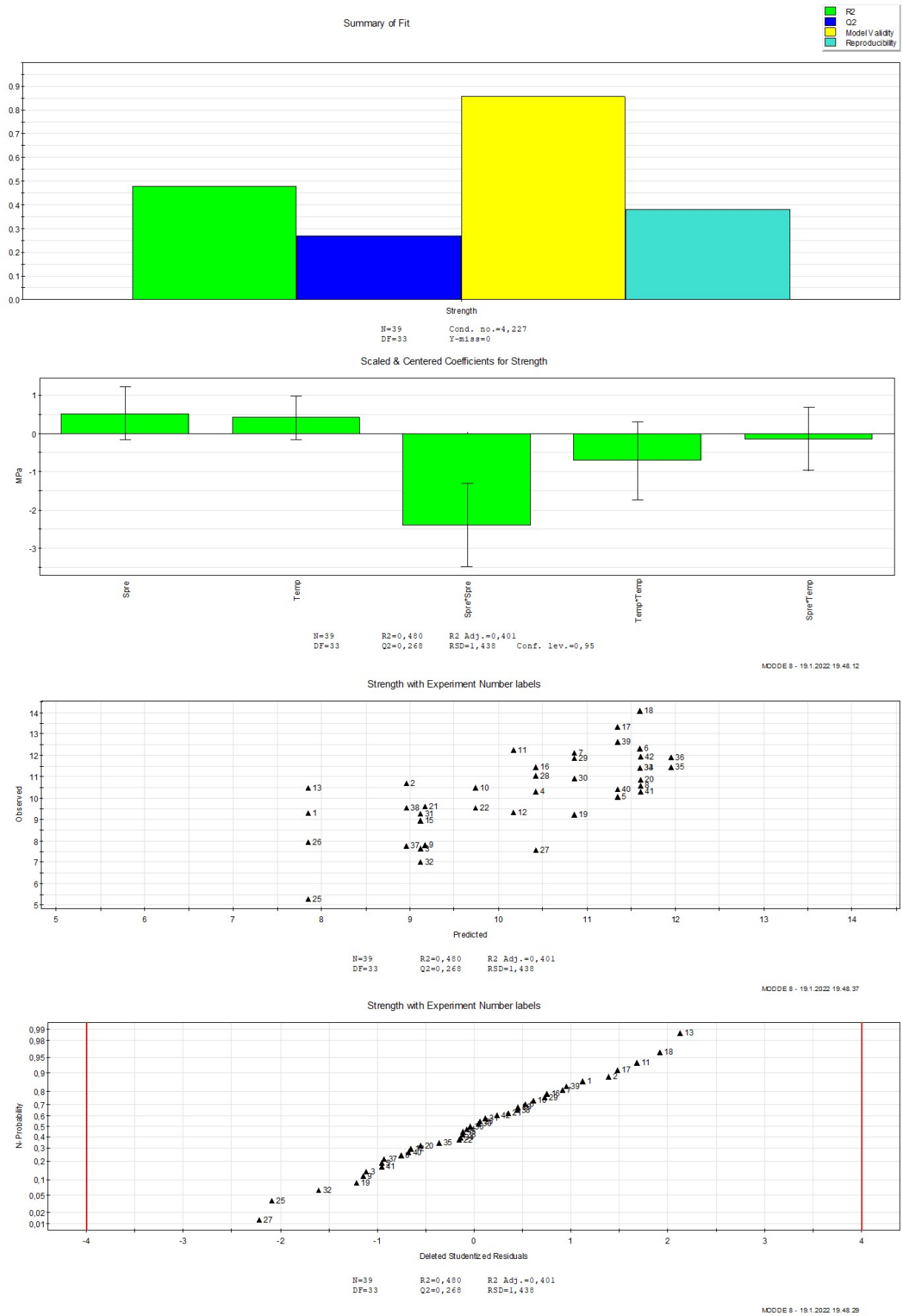


Fig. S21. Summary plot, coefficient plot, predicted versus occurred plot, and residual plot of Model 3.

## Supplementary Note 5: Thermal Characterization

Pans with pierced holes were used in the experiments to avoid rupture due to the pressure-buildup, which was observed at  $\sim 150$  °C when fully sealed pans were used, making the measurement more sensitive to signals from moisture evaporation and sorption. Because of this, there is a significant difference between the first and second scan cycles (Fig. S5). The first scans show a much larger endothermic region, suggesting moisture evaporation. The presence of moisture despite the measurement being performed right after freeze-drying is most likely due to water sorption onto lignin's hydroxyl and carbonyl groups.<sup>14-16</sup> The second cycle shows no sign of moisture evaporation or sorption, and therefore shows the differences between samples more clearly. EKL+LNP absorbs almost no heat in contrast to the other two samples, indicating high structural rigidity and low interpolymeric mobility.

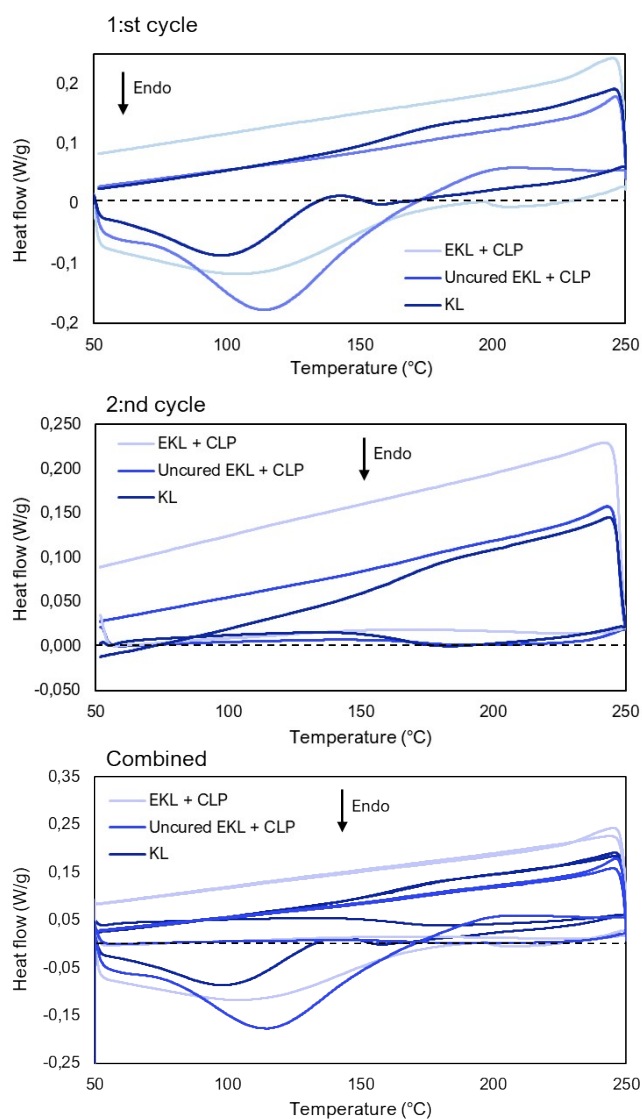


Fig. S22. DSC thermograms showing the 1:st and 2:nd cycle separately and combined.

## Supplementary Note 6: Lignin Particle Size and Surface charge

The size of the used LNPs was measured using dynamic light scattering (DLS). The reported Z-average size is the intensity-weighted mean size of the hydrodynamic diameter. The polydispersity index is a value from 0 – 1 which is dependent on the homogeneity of the particles and narrowness of the particle distribution, where small number indicate a narrow distribution.

Table S4. Average Z-size, polydispersity index (PDI) and Zeta potential of the used LNP dispersions.

Sample	Z-Size (nm)	PDI	Zeta-potential (mV)
Large	$770 \pm 5$	$0.04 \pm 0.03$	$-33.6 \pm 0.9$
Medium	$438 \pm 0.02$	$0.22 \pm 0.03$	$-37.9 \pm 0.9$
Small	$214 \pm 0.6$	$0.14 \pm 0.02$	$-35.2 \pm 0.9$

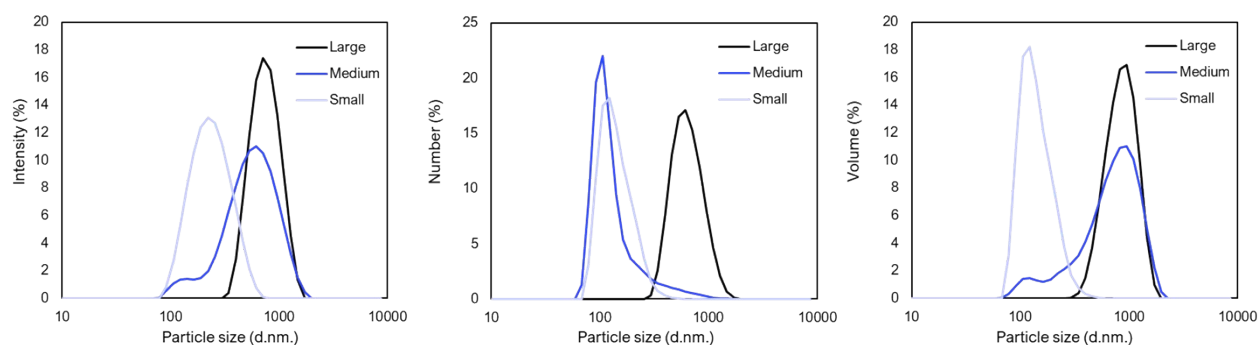


Fig. S23. Intensity, number, and volume particle size distribution of the used LNP dispersions.

## Supplementary Note 7: Estimation of operating cost

The operating costs of the EKL production plant was estimated to be 600 €/t. The distribution of the operating cost between raw materials, utilities and fixed operating costs can be seen in Fig. S24. The raw material feeds were retrieved from the mass balance and the utility consumption was estimated with Aspen Plus simulation software. The cost of lignin has been assumed to be the heating value of dry, purified lignin, when lignin has been used as energy instead of oil.<sup>17</sup> The fixed operating cost include such factors as personnel costs, administrative costs, maintenance, insurance and taxes.

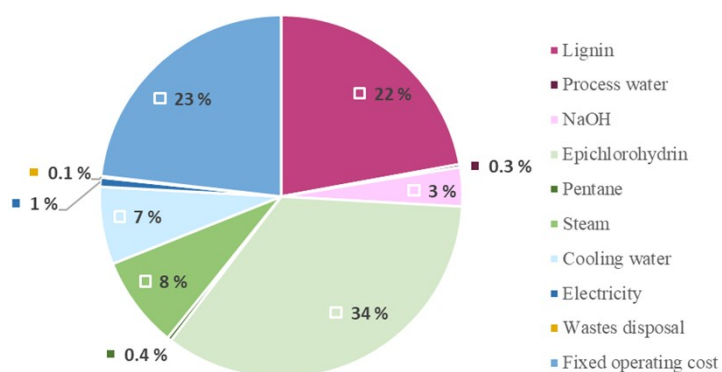


Fig. S24. The percentage distribution of the operating cost of EKL production plant.

## Supplementary Note 8: Life cycle assessment

The results are based on an assumption that all leftover process chemicals can be sold to a new location once the mill closes, so the calculations are made from only the chemical additions in the process. The Life Cycle Inventory data is collected in Table S5, and the life cycle assessment results are presented in Table S6.

Table S5. Life cycle assessment inventory data.

<b>Input/Process</b>	<b>Process data used</b>
<b>Water</b>	Europe without Switzerland: tap water production, conventional with biological treatment, ecoinvent 3.6 (agg)
<b>Electricity</b>	FI: electricity, high voltage, production mix, ecoinvent 3.6 (u-so)
<b>Steam</b>	RER: steam production, in chemical industry, ecoinvent 3.6 (u-so)
<b>Pentane</b>	RER: pentane production, ecoinvent 3.6 (agg)
<b>Sodium hydroxide</b>	CH: ethanol production from potatoes, ecoinvent 3.6 (agg)
<b>Epichlorohydrin</b>	RER: epichlorohydrin production from allyl chloride, ecoinvent 3.6 (agg)
<b>Transport</b>	RER: transport, freight, lorry >32 metric ton, EURO6, ecoinvent 3.6 (u-so)
<b>Lignin</b>	Bernier et Al. (2013) <sup>18</sup>
<b>Competing adhesives from renewable sources</b>	Arias et al. (2020) <sup>19</sup>
<b>Melamine-formaldehyde resin</b>	RER: melamine formaldehyde resin production, ecoinvent 3.6 (agg)
<b>Urea-formaldehyde resin</b>	RER: urea formaldehyde resin production, ecoinvent 3.6 (agg)
<b>Phenol-formaldehyde resin</b>	RER: phenolic resin production, ecoinvent 3.6 (agg)

Table S6. Life cycle assessment results.

<b>Input/Process</b>	<b>GWP standalone (kg CO<sub>2</sub>-eq.)</b>	<b>GWP integrated (kg CO<sub>2</sub>-eq.)</b>	<b>Fossil Depletion standalone (kg Oil-eq.)</b>	<b>Fossil Depletion Integrated (kg Oil-eq.)</b>
<b>Process Water</b>	10.2	10.2	4.8	4.8
<b>Cooling Water</b>	25.2	25.2	11.8	11.8
<b>Electricity</b>	35.9	3.6	28.8	2.9
<b>Steam</b>	1985.9	0	714.3	0
<b>Pentane</b>	16.0	16.0	25.2	25.2
<b>Sodium hydroxide</b>	314.0	314.0	111.2	111.2
<b>Epichlorohydrin</b>	633.9	633.9	275.3	275.3
<b>Transport</b>	22.5	9.5	8.5	3.6
<b>Lignin</b>	536.5	536.5	151.7	151.7
<b>Arias kraft</b>	8340.0	8340.0	2490	2490
<b>Arias soy</b>	2790.0	2790.0	1070	1070
<b>Arias tannin</b>	2970.0	2970.0	1180	1180
<b>MF resin</b>	4393.0	4393.0	1853.8	1853.8
<b>UF resin</b>	2481.1	2481.1	1184.5	1184.5
<b>PF resin</b>	3336.5	3336.5	2208.5	2208.5

To deal with uncertainties in the analysis, sensitivity analyses were performed. The variance was chosen as follows: Electricity consumption, -5% – 25%; heat consumption,  $\pm 5\%$ ; chemical consumption,  $\pm 5\%$ ; transport distance,  $\pm 50\%$ . The GWP impact from black liquor combustion is assumed here as zero. This is in line with the IPCC recommendation that all GWP impacts of biomass combustion needs to be fully included in the Agriculture, Forestry and Other Land-Use (AFOLU) sector.<sup>20</sup>

The removal of lignin from black liquor – and creating a new product from it – changes both the composition and heat value of black liquor which have a direct effect on pulp mill wide emissions. Often the black liquor heat transfer capacity of the recovery boiler is a bottle neck for pulp production at a mill. Removal of lignin from black liquor would therefore allow for an increased pulp production as the heat load is lowered in the recovery boiler.<sup>21</sup> This has several implications for the environmental impacts. Firstly, the overall mill production is increased as we have an increased pulp production and a new product from lignin. Secondly, the mill wide climate impact is increased as more woods need to be felled for the increased production. This impact needs to be allocated to the products to get a complete view of the environmental viability of the EKL process. These calculations nevertheless fall outside of this study's scope.

## References

1. Bryan, E. *Chemistry and Technology of Epoxy Resins*. London: Blackie Academic & Professional (1993). doi:10.1007/978-94-011-2932-9.
2. Alekhina, M., Ershova, O., Ebert, A., Heikkinen, S. & Sixta, H. Softwood kraft lignin for value-added applications: Fractionation and structural characterization. *Ind. Crops Prod.* **66**, 220–228 (2015).
3. Boeriu, C. G., Bravo, D., Gosselink, R. J. A. & Van Dam, J. E. G. Characterisation of structure-dependent functional properties of lignin with infrared spectroscopy. in *Industrial Crops and Products* vol. 20 205–218 (Elsevier, 2004).
4. Heitner, C., Dimmel, D. & Schmidt, J. *Lignin and Lignans: Advances in chemistry*. CRC Press Taylor & Francis Group (2010).
5. Stuart, B. H. *Infrared Spectroscopy: Fundamentals and Applications*. *Infrared Spectroscopy: Fundamentals and Applications* (2005). doi:10.1002/0470011149.
6. Ahvazi, B., Cloutier, É., Wojciechowicz, O. & Ngo, T. D. Lignin Profiling: A Guide for Selecting Appropriate Lignins as Precursors in Biomaterials Development. *ACS Sustainable Chemistry and Engineering* vol. 4 5090–5105 (2016).
7. Lu, Y. *et al.* Structural characterization of lignin and its degradation products with spectroscopic methods. *Journal of Spectroscopy* vol. 2017 (2017).
8. Salanti, A., Zoia, L. & Orlandi, M. Chemical modifications of lignin for the preparation of macromers containing cyclic carbonates. *Green Chem.* **18**, 4063–4072 (2016).
9. Gioia, C., Lo Re, G., Lawoko, M. & Berglund, L. Tunable Thermosetting Epoxies Based on Fractionated and Well-Characterized Lignins. *J. Am. Chem. Soc.* **140**, 4054–4061 (2018).
10. Zou, T., Sipponen, M. H., Henn, A. & Österberg, M. Solvent-Resistant Lignin-Epoxy Hybrid Nanoparticles for Covalent Surface Modification and High-Strength Particulate Adhesives. *ACS Nano* **15**, (2021).
11. Sipponen, M. H. *et al.* Spatially confined lignin nanospheres for biocatalytic ester synthesis in aqueous media. *Nat. Commun.* **9**, 2300 (2018).
12. Sipponen, M. H., Smyth, M., Leskinen, T., Johansson, L. S. & Österberg, M. All-lignin approach to prepare cationic colloidal lignin particles: Stabilization of durable Pickering emulsions. *Green Chem.* **19**, 5831–5840 (2017).
13. Meng, X. *et al.* Determination of hydroxyl groups in biorefinery resources via quantitative <sup>31</sup>P

- NMR spectroscopy. *Nat. Protoc.* **14**, 2627–2647 (2019).
14. Han, J., Zhou, C., Wu, Y., Liu, F. & Wu, Q. Self-assembling behavior of cellulose nanoparticles during freeze-drying: Effect of suspension concentration, particle size, crystal structure, and surface charge. *Biomacromolecules* **14**, 1529–1540 (2013).
  15. Farooq, M. *et al.* Well-Defined Lignin Model Films from Colloidal Lignin Particles. *Langmuir* **36**, 15592–15602 (2020).
  16. Guo, X., Yuan, H., Xiao, T. & Wu, Y. Application of micro-FTIR spectroscopy to study molecular association of adsorbed water with lignin. *Int. J. Biol. Macromol.* **131**, 1038–1043 (2019).
  17. Zhang, X. *et al.* Depolymerization of Kraft lignin into liquid fuels over a WO<sub>3</sub> modified acid-base coupled hydrogenation catalyst. *Fuel* **323**, 124428 (2022).
  18. Bernier, E., Lavigne, C. & Robidoux, P. Y. Life cycle assessment of kraft lignin for polymer applications. *Int. J. Life Cycle Assess.* **18**, 520–528 (2013).
  19. Arias, A., González-García, S., González-Rodríguez, S., Feijoo, G. & Moreira, M. T. Cradle-to-gate Life Cycle Assessment of bio-adhesives for the wood panel industry. A comparison with petrochemical alternatives. *Sci. Total Environ.* **738**, (2020).
  20. Eggleston, H. S., Buendia, L., Miwa, K., Ngara, T. & Tanabe, K. *2006 IPCC guidelines for national greenhouse gas inventories.* (2006).
  21. Vakkilainen, E. & Välimäki, E. Effect of lignin separation to black liquor and recovery boiler operation. in *TAPPI Press - TAPPI Engineering, Pulping and Environmental Conference 2009 - Innovations in Energy, Fiber and Compliance* vol. 3 (2009).